Short-Term Wind Speed and Direction Forecasting by 3DCNN and Deep Convolutional LSTM

Article *in* IEEJ Transactions on Electrical and Electronic Engineering · July 2022

DOI: 10.1002/tee.23669

6 authors, including:

Anggraini Puspita Sari
University of Pembangunan Nasional Veteran Jawa Timur
21 PUBLICATIONS **87** CITATIONS

SEE PROFILE

Dwi Arman Prasetya
Universitas Merdeka Malang
32 PUBLICATIONS **177** CITATIONS

SEE PROFILE

Rahman Arifuddin
Universitas Merdeka Malang
29 PUBLICATIONS **209** CITATIONS

SEE PROFILE

IEEJ TRANSACTIONS ON ELECTRICAL AND ELECTRONIC ENGINEERING
IEEJ Trans 2022; **17**: 1620–1628
Published online in Wiley Online Library (wileyonlinelibrary.com). DOI:10.1002/tee.23669

Paper

Short-Term Wind Speed and Direction Forecasting by 3DCNN and Deep Convolutional LSTM

Anggraini Puspita Sari[*,**a], Student Member
Hiroshi Suzuki[*], Member
Takahiro Kitajima[*], Member
Takashi Yasuno[*], Member
Dwi Arman Prasetya[**], Non-member
Rahman Arifuddin[***], Non-member

This paper investigates a deep learning-based wind-forecasting model to establish an accurate forecasting model which can support the increasing growth of wind power generation. The wind forecasting means wind speed and direction forecasting at the same time. Proposed forecasting model consists of three-dimensional convolutional neural network and deep convolutional long short-term memory (3DCNN-DConvLSTM), and forecasts the wind vector which expressed as time-sequential images. DConvLSTM model learns spatiotemporal features from time-series image data that represent a spatial and temporal change of wind speed and direction. The forecasting model combined of 3DCNN and DConvLSTM is effective to decrease training time, and forecasting error in comparison to the DConvLSTM model. Input of the forecasting model is wind speed and direction that is expressed as an image on 2D coordinate and uses the measured data by the Automated Meteorological Data Acquisition System (AMeDAS), Japan. Forecasting accuracy with one-hour ahead and its usefulness of the proposed forecasting model is evaluated with simulation results for four seasons that is typical of Japan climate, and demonstrated by comparison with fully connected-LSTM (FC-LSTM), encoder-decoder based 3DCNN (ED-3DCNN), DConvLSTM, and persistent models.

Keywords: wind power; wind speed forecasting; ConvLSTM; LSTM; CNN

Received 5 July 2021; Revised 1 June 2022

1. Introduction

All countries in the world have a common problem with stable and sustainable supply energy due to the consumption of energy increasing rapidly in accordance increasing population. One of the solutions to that problem is usage of renewable energy as alternative source energy. Renewable energy can also reduce greenhouse gas effects such as methane and carbon dioxide. The target of 2050 is to be able to supply 66% or two-third of the demand for energy on the world by usage of renewable energy [1].

Wind energy as friendly, green, and clean renewable energy has rapidly grown as an alternative resource and an important resource for electricity generation. Increased growth of the wind power generation is a potential and good impact for supply energy but has challenges about output power depends on wind speed and direction that cannot control, it is difficult to control stable the production of amount energy. To overcome it so necessary makes an accurate wind speed and direction forecasting to decrease unpredictability produced amount of energy later [1–3].

The wind forecasting method has three types: physical, statistical, and machine learning or artificial intelligence (AI) methods. Physical methods like the meso-scale model (MSM) and numerical weather prediction (NWP) is a good theory to get accurate forecasting but need accurate and full information about weather and atmospheric data and also need many computational costs [4,5]. Statistical methods such as Markov chain models, autoregressive (AR), AR moving average (ARMA), and AR integral MA (ARIMA) discovers a mathematical pattern to expressed wind time-series and good performance to learn linear features but poor to learn nonlinear features [3,6,7]. AI methods based on deep neural networks (DNN) such as multi-layer perceptron (MLP) and recurrent neural network (RNN) are great to learn nonlinear features, forecast the future of wind time-series, and locate the relationship between output data and input data without statistical method [4,6,7].

Much previous research uses neural network (NN), and forecast only wind speed by stacked denoising autoencoder (SDAE) [6],

[a] Correspondence to: Anggraini Puspita Sari. E-mail: sarianggraini15@gmail.com

[*]Department of Electrical and Electronic Engineering, Tokushima University, 2–1 Minami Josanjima Tokushima, 770–8506, Japan

[**]Department of Informatics, Universitas Pembangunan Nasional "Veteran", Jawa Timur Jl. Raya Rungkut Madya Gunung Anyar Surabaya 60–294, Indonesia

[***]Department of Electrical Engineering, University of Merdeka Malang Jl, Taman Agung 1 Malang, 65–146, Indonesia

convolutional neural network (CNN) [4], long short-term memory-recurrent neural network (LSTM-RNN) [3], and so on. This paper proposes a novel forecasting model of both wind speed and direction (wind information) at the same time by the AI method using three-dimensional CNN-deep convolutional long short-term memory (3DCNN-DConvLSTM) which combining encoder-decoder based 3DCNN (ED-3DCNN) and deep ConvLSTM (DConvLSTM). DConvLSTM analyzes time-series image data including wind information and extracts spatiotemporal features of wind information. On the other hand, ED-3DCNN uses encoder and decoder networks to extract spatial and temporal features. DConvLSTM between encoder and decoder networks is used to improve forecasting accuracy, be easy for training, and decrease training time [8,9].

Wind information is acquired from Automated Meteorological Data Acquisition System (AMeDAS) at 1 h interval in Tokushima city, Japan. Effectiveness of the proposed forecasting model for a short-term forecasting that is 1 h ahead demonstrate by several simulation results for each season in 1 year which is conducted for the purpose of comparing with fully connected - long short-term memory (FC-LSTM), ED-3DCNN, DConvLSTM, and persistent models. Performances of all forecasting models are summarized and evaluated using mean absolute error (MAE), root mean square error (RMSE), and mean bias error (MBE).

2. Proposed Models

2.1. Data set Wind information from AMeDAS is expressed by wind speed v (m/s) and 16 directions as shown in Fig. 1(a). In our proposed forecasting model, wind information is provided as images. The wind speed and direction are resolved into east (E)-west (W) and north (N)-south (S) components. $v_x(t)$ and $v_y(t)$ [m/s] as shown in Fig. 1(b). These components are calculated by

$$v_x(t) = v(t)\cos\gamma(t) \tag{1}$$

$$v_y(t) = v(t)\sin\gamma(t) \tag{2}$$

where $\gamma(t)$ is wind direction [°] calculated from 16 directions.

In order for effective use of the image processing capability of deep learning algorithm, wind information is plotted to image and used for input and output data of the model. Size of input and output images are 128 × 128 pixel. The wind information is

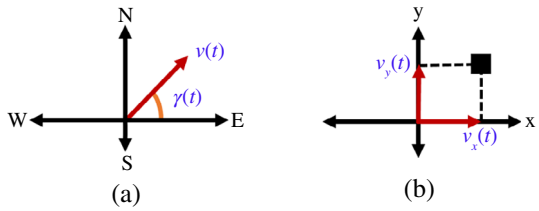

Fig. 1. Wind speed and direction on coordinate system (a) vector diagram (b) definition of component $v(t)$

plotted to a point $(p_x(t), p_y(t))$ in the image by python imaging library (PIL) by using following conversion formula,

$$p_x(t) = \frac{64}{20}v_x(t) + 64 \tag{3}$$

$$p_y(t) = 64 - \frac{64}{20}v_y(t) \tag{4}$$

where 64 is half of image size and 20 means estimated maximum wind speed 20 (m/s). The reason the maximum scale is 20 m/s that is the maximum wind speed of Tokushima city by AMeDAS from December 2014 to November 2018 is approaching 20 m/s that is 19.8 m/s as shown in Table I. The wind speed is 10 min averaged data. In addition, it is easy to predict that the wind speed will be high when a typhoon approaches. In addition, the wind power generator will be stopped for safety, so the demand for wind speed forecast at typhoon is not high. In this paper, we set the value that wind speed does not exceed the estimated maximum wind speed which depends on the historical wind information in the city. In order to express information of wind speed change, the input image contains six plotted points at $p(t-5)$ to $p(t)$ which represent 6 h data. The six points are connected by line and the latest point is larger than the others. Figure 2 shows procedure of the input image generation. Moreover, the input data are time sequenced nine images from $m(t-8)$ to $m(t)$ as shown in Fig. 2. Table II shows a period of data set for test, validation, and training. The time sequence of the output image is the same as the input image is shown in Fig. 3. From Fig. 3, the target image of 1 h ahead is the last image (ninth image) of the output and the other eight images are past time data. The effect of the eight images in the output images is to improve forecast error by taking the most recent wind speed change into account.

Table I. Maximum wind speed every month

Month	December 2014–November 2015	December 2015–November 2016	December 2016–November 2017	December 2017–November 2018
December	8.5	9.7	9.5	8.3
January	9.8	9.6	9.5	8.2
February	9.9	10.3	9.9	12.8
March	9.4	8.6	9.2	9.4
April	9.5	10.9	10.2	9.4
May	11.7	13.2	8.3	9.2
June	9.5	8.9	10.4	8.4
July	17.8	7.7	6.7	12.7
August	15.9	8	12.4	12.6
September	7.4	12	19.8	16
October	9.6	8.1	9.7	12.4
November	8.3	9.2	8.5	7.8

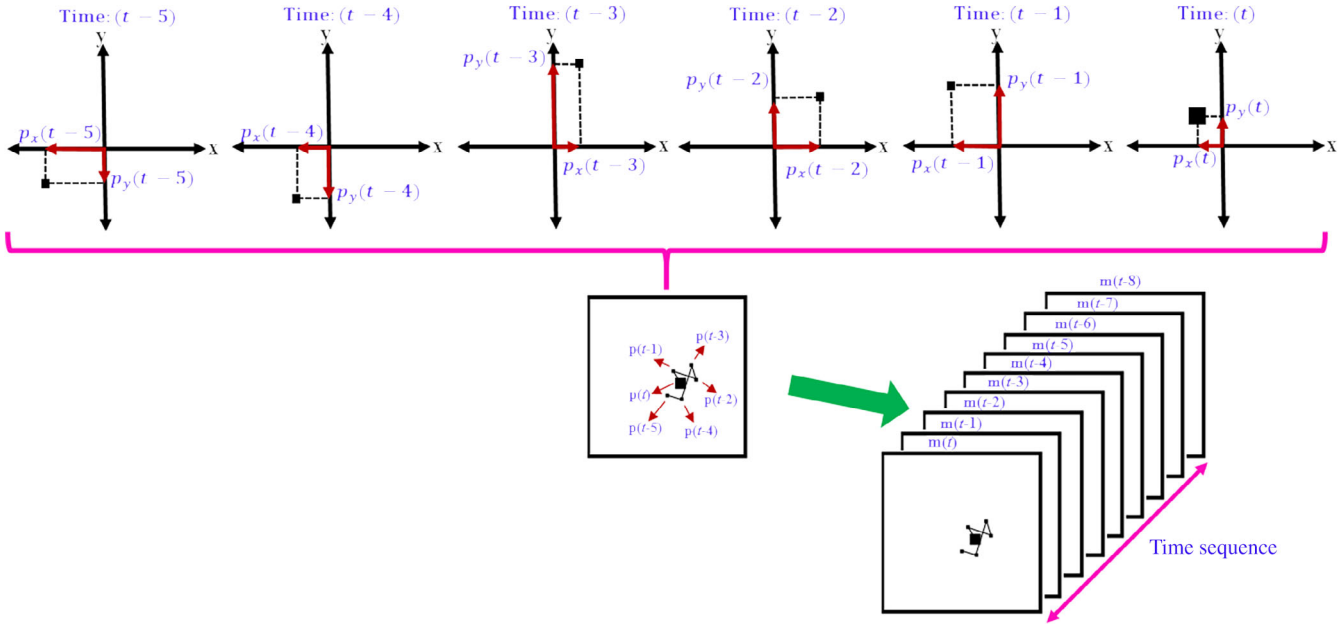

Fig. 2. Procedure of input image generation

Table II. Period of data set

Data set	Period
Training	December 2014–November 2016
Validation	December 2016–November 2017
Test	December 2017–November 2018

2.2. FC-LSTM LSTM is an advanced kind of RNN and a very famous model for analyzing time-series data. Furthermore, LSTM is powerful and stable to learn long-term dependency which is realized by three gates: input, forget, and output gates. This paper uses FC-LSTM that is strong for learning temporal relationship and it affects the loss of spatial information. All states and gates of FC-LSTM are 1D vectors [10–12]. The network of FC-LSTM consists of four LSTM layers and one fully connected (FC) layer. Each LSTM layer uses 32 units which are the same number of channel size in the ConvLSTM layer. The last FC layer is used to get forecasted result. The important equation of LSTM unit are follows [10,11,13],

$$\boldsymbol{i}_t = \sigma\left(\boldsymbol{W}_{xi} \cdot \boldsymbol{x}_t + \boldsymbol{W}_{Hi} \cdot \boldsymbol{H}_{t-1} + \boldsymbol{W}_{Ci} \circ \boldsymbol{C}_{t-1} + b_i\right) \tag{5}$$

$$\boldsymbol{C}_t = \boldsymbol{f}_t \circ \boldsymbol{C}_{t-1} + \boldsymbol{i}_t \circ \tanh\left(\boldsymbol{W}_{xC} \cdot \boldsymbol{x}_t + \boldsymbol{W}_{HC} \cdot \boldsymbol{H}_{t-1} + b_C\right) \tag{6}$$

$$\boldsymbol{f}_t = \sigma\left(\boldsymbol{W}_{xf} \cdot \boldsymbol{x}_t + \boldsymbol{W}_{Hf} \cdot \boldsymbol{H}_{t-1} + \boldsymbol{W}_{Cf} \circ \boldsymbol{C}_{t-1} + b_f\right) \tag{7}$$

$$\boldsymbol{o}_t = \sigma\left(\boldsymbol{W}_{xo} \cdot \boldsymbol{x}_t + \boldsymbol{W}_{Ho} \cdot \boldsymbol{H}_{t-1} + \boldsymbol{W}_{Co} \circ \boldsymbol{C}_t + b_o\right) \tag{8}$$

$$\boldsymbol{H}_t = \boldsymbol{o}_t \circ \tanh\left(\boldsymbol{C}_t\right) \tag{9}$$

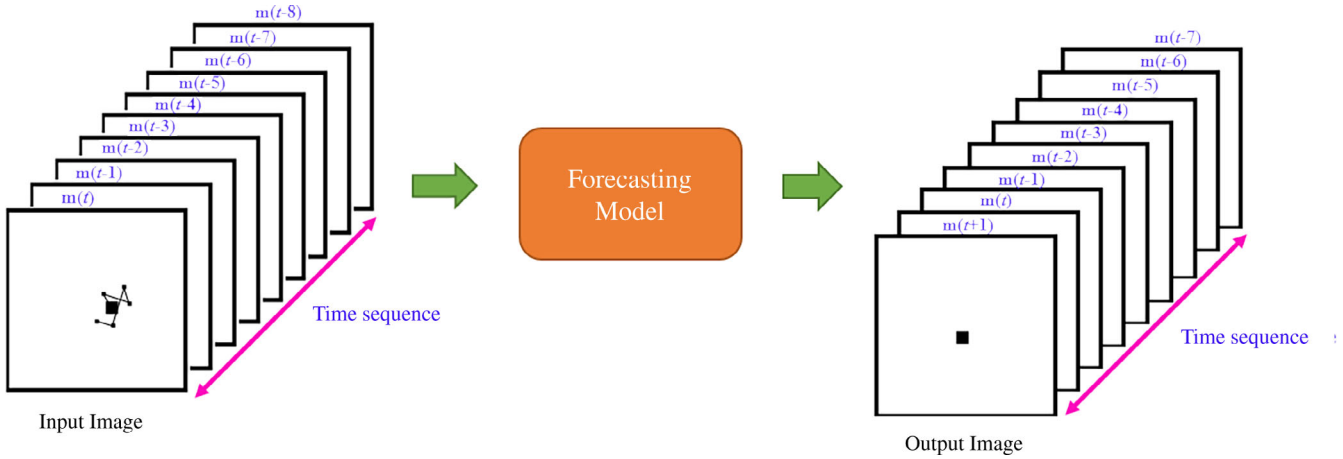

Fig. 3. Input and output image components of forecasting model

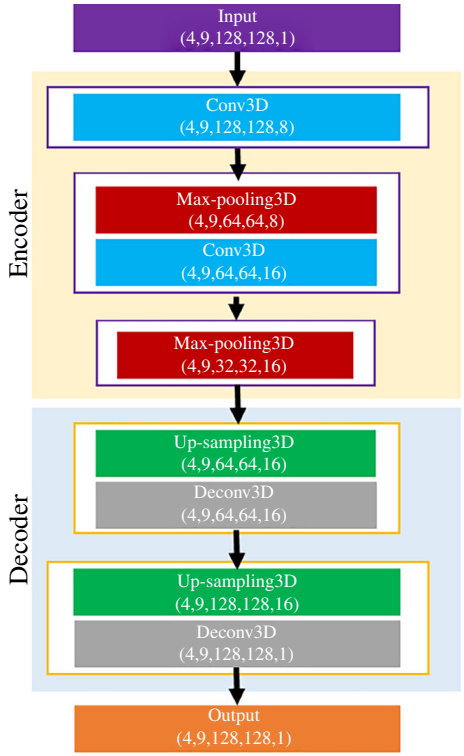

Fig. 4. Configuration of ED-3DCNN model

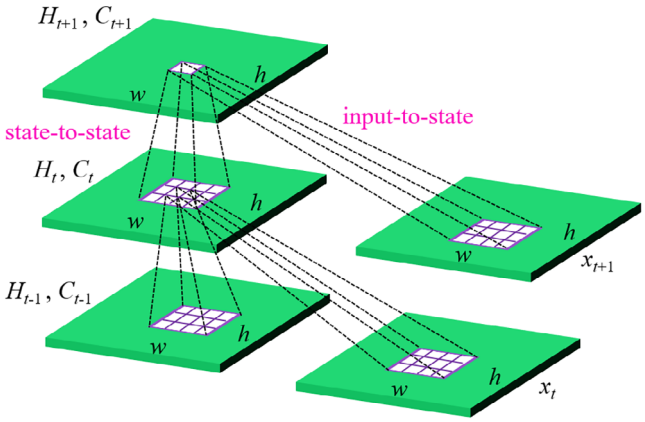

Fig. 5. Internal structure of ConvLSTM

Fig. 6. Configuration of DConvLSTM model

where $\boldsymbol{W}$ is weight, b is bias, $\boldsymbol{H}$ is hidden state, $\boldsymbol{x}$ is input data, σ is activation function, $\circ$ is Hadamard product, $\boldsymbol{i}$, $\boldsymbol{C}$, $\boldsymbol{f}$, $\boldsymbol{o}$ mean input gate, cell state, forget gate, and output gate, respectively.

2.3. ED-3DCNN CNN is a suitable and efficient method to process the images (2DCNN), video (3DCNN), and sounds (1DCNN) [9,14]. This paper uses ED-3DCNN which consists of encoder and decoder networks as shown in Fig. 4. Encoder-decoder based 3DCNN has five-dimensional feature maps: number of sample data (N), depth (d), height (h), width (w), and channel (c) [15]. The encoder network consists of two Conv layers and two max-pooling layers that convolute spatial and temporal dimensions, and also output narrowed feature maps. The decoder network consists of two Deconv layers and two up-sampling layers that reconstitute image from feature maps enlarged h and w. The kernel size is five. The channel sizes of Conv are 8 and 16. The channel sizes of Deconv are 16 and 1. The reason for the end process of Deconv utilizes one channel to get the forecasted result.

2.4. DConvLSTM ConvLSTM model for improvement of LSTM model which is used convolutional structure for both transitions; state-to-state and input-to-state so that can receive five dimensions [N, time sequence (ts), h, w, and c] as shown in Fig. 5 can accomplish sequence to sequence process [10,11].

Moreover, equation of ConvLSTM uses a convolution operation '$\star$' by replaced product operation '$\cdot$' in equations of LSTM ((5)–(9)) as shown in (10)–(14) [8,10,11,13],

$$\boldsymbol{i}_t = \sigma\left(\boldsymbol{W}_{xi} \star \boldsymbol{x}_t + \boldsymbol{W}_{Hi} \star \boldsymbol{H}_{t-1} + \boldsymbol{W}_{Ci} \circ \boldsymbol{C}_{t-1} + b_i\right) \tag{10}$$

$$\boldsymbol{f}_t = \sigma\left(\boldsymbol{W}_{xf} \star \boldsymbol{x}_t + \boldsymbol{W}_{Hf} \star \boldsymbol{H}_{t-1} + \boldsymbol{W}_{Cf} \circ \boldsymbol{C}_{t-1} + b_f\right) \tag{11}$$

$$\boldsymbol{C}_t = \boldsymbol{f}_t \circ \boldsymbol{C}_{t-1} + \boldsymbol{i}_t \circ \tanh\left(\boldsymbol{W}_{xC} \star \boldsymbol{x}_t + \boldsymbol{W}_{HC} \star \boldsymbol{h}_{t-1} + b_C\right) \tag{12}$$

$$\boldsymbol{o}_t = \sigma\left(\boldsymbol{W}_{xo} \star \boldsymbol{x}_t + \boldsymbol{W}_{Ho} \star \boldsymbol{H}_{t-1} + \boldsymbol{W}_{Co} \circ \boldsymbol{C}_t + b_o\right) \tag{13}$$

$$\boldsymbol{H}_t = \boldsymbol{o}_t \circ \tanh\left(\boldsymbol{C}_t\right) \tag{14}$$

Similarly that LSTM, ConvLSTM has cell state, forget gate, input gate, and output gate.

This paper proposes the multilayer ConvLSTM that uses four ConvLSTM layers in both networks: encoder network and forecaster network that is called the DConvLSTM (Deep ConvLSTM) model for spatiotemporal sequence forecasting as shown in Fig. 6. Encoder network consists of ConvLSTM layer, and forecaster network consists of ConvLSTM layer and a Conv layer. Fore inputs to the forecaster network are set to zero arrays.

Channel size of ConvLSTM layers are 32. The kernel size is five. In the forecaster network, state of the ConvLSTM layer are copied out of the last state of the ConvLSTM layer in the encoder network. The end process of the DConvLSTM model executes sequence to sequence use the Conv layer for capturing spatiotemporal features from the ConvLSTM layer in the forecaster network. The input and output of the DConvLSTM model are the same sizes. The all-states of DConvLSTM concatenate in the forecaster network to input of Conv layer that it uses channel size one for getting forecasting results.

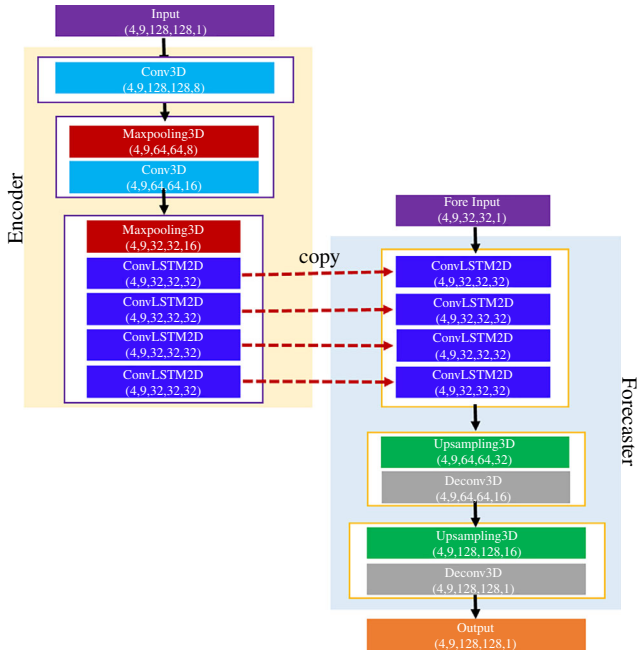

Fig. 7. Configuration of 3DCNN-DConvLSTM model

2.5. 3DCNN-DConvLSTM 3DCNN-DConvLSTM is combines ED-3DCNN and DConvLSTM models. 3DCNN-DConvLSTM is the forecasting model improved DConvLSTM model which combines the merit of CNN and ConvLSTM: can improve forecasting accuracy, reduce training time, and more easily to training. The reason 3DCNN-DConvLSTM can easy to training: the feature maps narrowed use max-pooling layer so can easy to train in ConvLSTM layer and output can get same size using up-sampling layer. Configuration of 3DCNN-DConvLSTM model is shown in Fig. 7.

3DCNN-DConvLSTM model consists of encoder and forecaster networks. Encoder network composes of two Conv layers, two max-pooling layers, and four ConvLSTM layers. In encoder network, max-pooling used to narrowed h and w of feature maps. Forecaster network composes of two Deconv layers, two up-sampling layers, and four ConvLSTM layers that is feature maps are enlarged h and w by up-sampling. Fore input uses zero arrays. Fore input required as input in the forecaster network and it to copy the last state from ConvLSTM layer in the encoder network to ConvLSTM layer in the forecaster network for getting output image. Channel size of two Conv and two Deconv layers are 8, 16, 16, and 1, respectively. The end Deconv is one layer and outputs the forecasting result. The channel size of ConvLSTM is 32. The kernel size of Conv., Deconv. and ConvLSTM layers use five. The procedure of the 3DCNN-DConvLSTM model is similar to the DConvLSTM model but the difference the DConvLSTM is located between 3DCNNs.

2.6. Learning procedures Table III shows the learning conditions of the proposed forecasting models. Leaky ReLU (Leaky rectified linear unit) is employed as an activation function for resolving dying ReLU that has a non-zero slope part and can speed up training time. The training process is iterated for 20 epochs with batch size four. The network is trained using RMSProp (root mean square propagation) optimizer.

Table III. Learning condition of proposed models

Description	Data		
Activation function	Leaky ReLU		
Epoch	20		
Batch size	4		
Optimizer	RMSProp	lr	0.001
		ρ	0.9

Performances of the proposed forecasting models are evaluated by *MAE*, *RMSE*, and *MBE* these evaluation indexes are defined as,

$$MAE = \frac{1}{N}\sum_{r=1}^{N} \mid y_r - \widehat{y}_r \mid \tag{15}$$

$$RMSE = \sqrt{\frac{1}{N}\sum_{r=1}^{N}(y_r - \widehat{y}_r)^2} \tag{16}$$

$$MBE = \frac{1}{N}\sum_{r=1}^{N}(\widehat{y}_r - y_r) \tag{17}$$

where N means the number of learning data, y_r means actual measurement data, and $\widehat{y}_r$ means forecasted data. *RMSE* is suitable for evaluating the overall accuracy of the forecasts while penalizing large forecast errors in a square order. *RMSE* is obtained for minimizing squared errors so that lead to forecasting of the mean. *MAE* is suitable for evaluating uniform forecast errors. *MAE* is obtained for minimizing absolute average error that measure the closeness of the forecasting to actual measurement data so that lead to forecasting of the median. *MBE* is suitable for assessing forecast bias [16,17].

3. Forecasted Results

Forecasted results (wind speed and direction) are extracted from the forecasting of image as a center of gravity position of the largest pixel cluster with value zero. The forecasted position is converted to $\widehat{v}_x(t)$ and $\widehat{v}_y(t)$ with substracted the center position of the image (64, 64) that are calculated $\widehat{p}_x(t)$ and $\widehat{p}_y(t)$ as follows,

$$\widehat{v}_x(t) = \frac{20}{64}(\widehat{p}_x(t) - 64) \tag{18}$$

$$\widehat{v}_y(t) = \frac{20}{64}\left(64 - \widehat{p}_y(t)\right) \tag{19}$$

Forecasted wind speed and direction are calculated by

$$\widehat{\gamma}(t) = \tan^{-1}\left(\frac{\widehat{v}_y(t)}{\widehat{v}_x(t)}\right) \tag{20}$$

$$\widehat{v}(t) = \sqrt{\widehat{v}_x^2(t) + \widehat{v}_y^2(t)} \tag{21}$$

where $\widehat{\gamma}(t)$ is forecasted wind direction [°], and $\widehat{v}(t)$ is forecasted wind speed (m/s).

Figures 8 and 9 show forecasted results of wind speed and direction for 1-day in November 25, 2018, respectively. The reason for choosing November because the RMSE is lower than other months and for choosing date 25 due to the rapid influence change of wind speed and direction to all forecasting models.

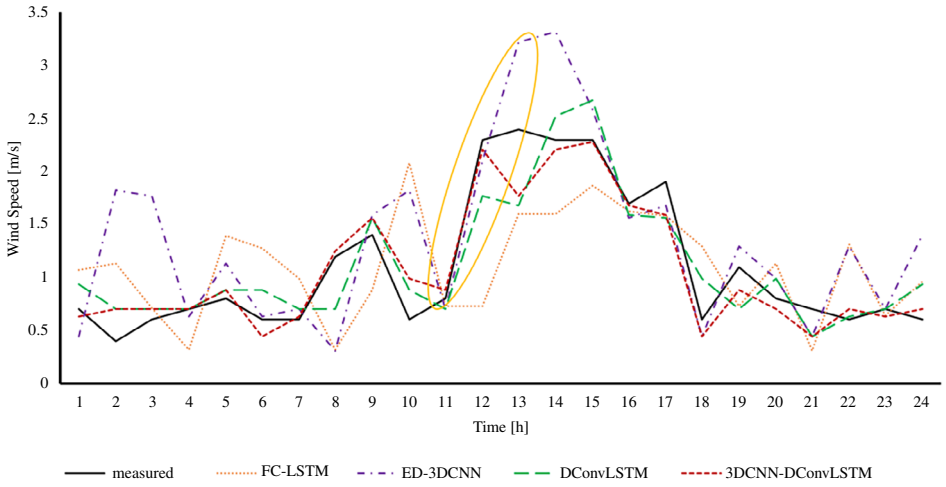

Fig. 8. Forecasted results of wind speed on November 25, 2018

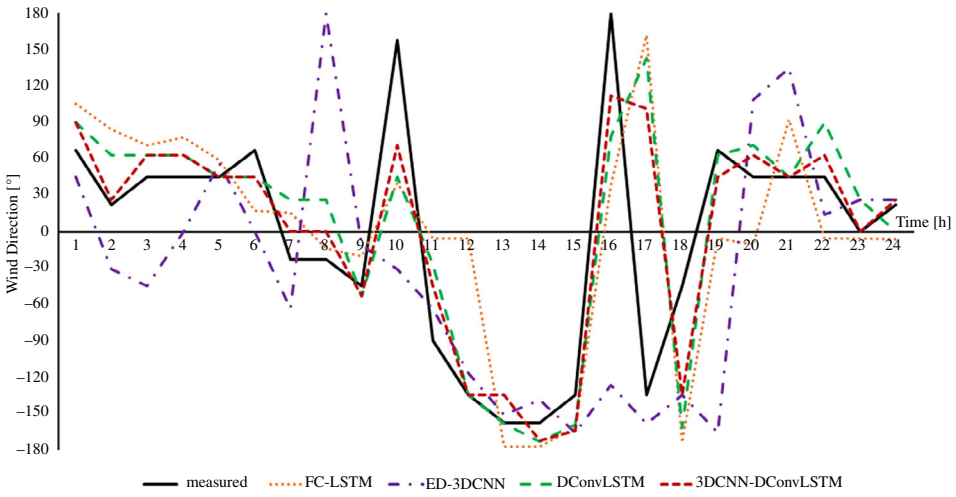

Fig. 9. Forecasted results of wind direction on November 25, 2018

For confirming the effectiveness of 3DCNN-ConvLSTM model, we compare with FC-LSTM, ED-3DCNN, DConvLSTM, and Persistent models. From Fig. 8 (yellow oval mark), in cases of DConvLSTM and 3DCNN-DConvLSTM, the forecasting delay caused rapidly change of wind speed was reduced than FC-LSTM. That is, it was confirmed that DConvLSTM and 3DCNN-DConvLSTM models can effectively extract temporal features of wind vector change due to the expression of wind vector transition on 2D image. From Figs 8 and 9, forecasted wind speed and direction by the proposed 3DCNN-DConvLSTM model is approached measured data compared with other forecasting models.

Tables IV–VI show values of RMSE, MAE, MBE used for evaluation of each forecasting models. For calculating MAE uses the absolute value for evaluation, in that case, forecasting errors have a small variance that caused MAE is slightly lower than RMSE. In Tables IV and V, the FC-LSTM model has the lowest forecasting accuracy for wind speed and forecasting accuracy for the wind speed of the ED-3DCNN model better than the FC-LSTM model. From Table IV, the FC-LSTM model has the lowest forecasting accuracy for a total wind direction, and the ED-3DCNN model slightly better than the FC-LSTM model. From Table V, the ED-3DCNN model has the lowest forecasting accuracy for a total wind direction, and the FC-LSTM model slightly better than the ED-3DCNN model. DConvLSTM and 3DCNN-DConvLSTM models can be improving accuracy than FC-LSTM and ED-3DCNN which the highest forecasting accuracy is 3DCNN-DConvLSTM in RMSE and MAE so the 3DCNN-DConvLSTM model is the best forecasting model than other models. Positive value of MBE representing error of forecasting model to overestimation and negative value of MBE representing error of forecasting model to underestimated while positive value of MBE to wind direction representing clockwise deviation and conversely. From Table VI of wind speed, the total MBE value of 3DCNN-DConvLSTM, DCLSTM, persistent model, and FC LSTM are negative values and MBE of ED-3DCNN is positive value. From Table VI of wind direction, the total MBE value of all models are positive values.

Table VII shows the improvement rate of DConvLSTM and 3DCNN-DConvLSTM models over FC-LSTM model from December 2017 to November 2018. From RMSE column of Table VI, DConvLSTM can improve the accuracy of wind speed

Table IV. RMSE of wind speed and direction

Description		RMSE				
		FC-LSTM	ED-3DCNN	DConvLSTM	Persistent model	3DCNN-DConvLSTM
December	v (m/s)	1.37	1.23	1.08	1.28	**1.04**
	γ (°)	37.6	40.8	36.0	37.6	**33.0**
January	v (m/s)	1.43	1.27	1.07	1.28	**1.02**
	γ (°)	41.3	43.5	40.1	42.2	**35.6**
February	v (m/s)	1.55	1.26	1.05	1.25	**1.03**
	γ (°)	45.0	44.7	44.1	48.6	**40.9**
March	v (m/s)	1.59	1.26	1.10	1.33	**1.07**
	γ (°)	56.1	56.7	49.6	57.2	**47.4**
April	v (m/s)	1.72	1.29	1.20	1.43	**1.15**
	γ (°)	58.9	57.1	51.3	60.2	**49.0**
May	v (m/s)	1.56	1.21	1.15	1.42	**1.10**
	γ (°)	61.9	61.7	54.6	64.6	**52.5**
June	v (m/s)	1.46	1.18	1.05	1.25	**0.99**
	γ (°)	55.8	52.2	52.0	57.7	**47.1**
July	v (m/s)	1.88	1.32	1.12	1.31	**1.08**
	γ (°)	52.1	50.1	47.2	56.4	**46.7**
August	v (m/s)	1.71	1.23	1.11	1.22	**1.04**
	γ (°)	53.5	48.4	48.2	56.6	**44.1**
September	v (m/s)	2.06	1.30	1.15	1.44	**1.12**
	γ (°)	56.4	58.7	54.9	56.6	**48.2**
October	v (m/s)	1.49	1.20	1.07	1.24	**1.02**
	γ (°)	45.6	48.9	43.5	46.3	**40.2**
November	v (m/s)	1.15	1.08	0.89	0.95	**0.85**
	γ (°)	38.9	41.7	35.7	39.6	**32.8**
Total	v (m/s)	1.60	1.24	1.09	1.29	**1.05**
	γ (°)	50.9	50.9	46.9	52.7	**43.6**

Note: Bold values are the best forecasting result of 3DCNN-ConvLSTM than other models.

Table V. MAE of wind speed and direction

Description		MAE				
		FC-LSTM	ED-3DCNN	DConvLSTM	Persistent model	3DCNN-DConvLSTM
December	v(m/s)	1.06	0.98	0.83	0.99	**0.81**
	γ (°)	23.1	25.6	22.2	23.6	**20.1**
January	v(m/s)	1.10	0.99	0.82	0.95	**0.77**
	γ (°)	26.0	26.4	24.2	25.4	**21.5**
February	v(m/s)	1.13	0.99	0.79	0.94	**0.78**
	γ (°)	29.1	29.9	27.9	31.5	**25.7**
March	v (m/s)	1.16	0.95	0.79	0.95	**0.78**
	γ (°)	37.4	37.9	32.5	38.2	**30.6**
April	v (m/s)	1.29	0.97	0.89	1.07	**0.87**
	γ (°)	40.0	37.5	33.5	40.3	**31.9**
May	v (m/s)	1.17	0.91	0.84	1.03	**0.79**
	γ (°)	42.5	41.7	36.5	44.3	**34.7**
June	v (m/s)	1.12	0.89	0.79	0.95	**0.74**
	γ (°)	37.1	35.1	33.9	38.3	**30.2**
July	v (m/s)	1.38	1.03	0.85	1.01	**0.83**
	γ (°)	33.4	32.2	29.2	35.7	**28.6**
August	v (m/s)	1.26	0.90	0.80	0.91	**0.75**
	γ (°)	34.8	31.5	30.6	36.3	**27.5**
September	v(m/s)	1.29	0.95	0.84	0.98	**0.79**
	γ (°)	38.2	39.9	35.8	38.2	**31.5**
October	v(m/s)	1.05	0.93	0.81	0.91	**0.76**
	γ (°)	30.0	32.9	28.4	30.8	**26.3**
November	v(m/s)	0.87	0.84	0.68	0.74	**0.65**
	γ (°)	24.9	27.1	22.5	25.4	**21.1**
Total	v(m/s)	1.16	0.95	0.81	0.95	**0.78**
	γ (°)	33.1	33.2	29.8	34.0	**27.5**

Note: Bold values are the best forecasting result of 3DCNN-ConvLSTM than other models.

Table VI. MBE of wind speed and direction

Description		MBE				
		FC-LSTM	ED-3DCNN	DConvLSTM	Persistent model	3DCNN-DConvLSTM
December	v (m/s)	−0.53	0.09	−0.21	−0.03	−0.02
	γ (°)	14.1	8.11	10.1	11.4	6.18
January	v(m/s)	−0.39	0.18	−0.17	−0.05	−0.05
	γ (°)	13.7	8.45	9.11	10.4	6.68
February	v(m/s)	−0.56	0.10	−0.21	−0.10	−0.08
	γ (°)	17.5	9.92	9.96	11.6	8.64
March	v(m/s)	−0.70	0.08	−0.15	−0.14	−0.15
	γ (°)	18.7	14.2	8.39	10.7	6.17
April	v (m/s)	−0.79	−0.07	−0.19	−0.19	−0.19
	γ (°)	18.6	13.6	11.0	8.41	5.74
May	v (m/s)	−0.61	0.01	−0.16	−0.19	−0.19
	γ (°)	17.1	13.9	10.1	8.08	3.24
June	v (m/s)	−0.51	−0.01	−0.19	−0.16	−0.17
	γ (°)	15.8	12.4	10.1	9.84	4.46
July	v (m/s)	−0.74	−0.06	−0.08	−0.22	−0.22
	γ (°)	6.20	10.0	7.06	8.49	5.06
August	v (m/s)	−0.74	−0.01	−0.08	−0.19	−0.19
	γ (°)	11.6	5.72	5.98	9.34	6.24
September	v (m/s)	−0.71	0.04	−0.21	−0.11	−0.10
	γ (°)	17.5	11.7	9.77	10.9	7.54
October	v (m/s)	−0.54	0.14	−0.17	−0.03	−0.04
	γ (°)	18.9	11.2	11.1	14.6	10.3
November	v (m/s)	−0.36	0.12	−0.20	0.02	0.01
	γ (°)	11.7	3.91	5.26	9.27	4.61
Total	v (m/s)	−0.60	0.05	−0.17	−0.12	−0.12
	γ (°)	15.1	10.3	8.98	10.2	6.23

is 21.46%–44.02% and wind direction is 2.02%–13.06% and also 3DCNN-DConvLSTM can improve accuracy of wind speed is 23.90%–45.70% and wind direction is 9.20%–17.70%. Similarly, from MAE column of Table VII, DConvLSTM can improve the accuracy of wind speed is 21.01%–38.35% and wind direction is 3.59%–16.24% and also 3DCNN-DConvLSTM can improve accuracy of wind speed is 23.52%–40.52% and wind direction is 11.67%–21.09%. From Table VII, the 3DCNN-ConvLSTM model can improve accuracy than DConvLSTM, significantly both in wind speed and direction that it indicates 3DCNN-ConvLSTM is the benchmark model.

Training time of all forecasting models are shown in Fig. 10. The training time shown in Fig. 10 is the time required to train 2 years of data. DConvLSTM model is the longest training time and ED-3DCNN model is the shortest training time. From these result, we can confirm that 3DCNN-DConvLSTM model can effectively reduce training time of DConvLSTM model. This is due to have process max-pooling to narrow feature maps before ConvLSTM process that can be easy to training, after ConvLSTM process, we use up-sampling to enlarge feature maps so get same size of input and output image. Overall, 3DCNN-DConvLSTM model can achieve the best forecasting accuracy, and effectively decrease training time than DConvLSTM, and it indicates the best forecasting model. The forecasting data uses 1 year and the forecasting time is a quarter of training time due to the forecasting process not needing backpropagation calculation. So that, the forecasting time to each model forecast 1 h ahead get from quotient between forecasting time for 1 year and amount of data 1 year and it as shown in Table VIII.

Table VII. Improvement rate of wind speed and direction

Description		Improvement rate (%) RMSE DConvLSTM	RMSE 3DCNN-DConvLSTM	MAE DConvLSTM	MAE 3DCNN-DConvLSTM
December	v (m/s)	21.5	23.9	21.0	23.5
	γ (°)	4.05	12.1	3.59	12.7
January	$v(t)$ (m/s)	25.2	28.2	25.5	30.3
	γ (°)	2.72	13.8	6.85	17.4
February	v (m/s)	32.3	33.5	29.5	31.2
	γ (°)	2.02	9.20	3.98	11.7
March	v(m/s)	30.9	32.5	31.5	32.5
	γ (°)	11.6	15.4	13.1	18.3
April	v (m/s)	29.8	33.0	30.7	32.8
	γ (°)	13.1	16.9	16.2	20.1
May	v (m/s)	26.3	29.4	28.5	32.1
	γ (°)	11.9	15.1	14.1	18.3
June	v (m/s)	28.1	31.6	29.5	34.2
	γ (°)	6.77	15.5	8.33	18.3
July	v (m/s)	40.5	42.4	38.4	40.1
	γ (°)	9.33	10.3	12.3	14.3
August	v (m/s)	34.7	38.9	36.4	40.5
	γ (°)	10.0	17.7	12.3	21.1
September	v (m/s)	44.0	45.7	35.3	38.8
	γ (°)	2.64	14.5	6.3	17.5
October	v (m/s)	28.5	32.0	23.0	27.4
	γ (°)	4.59	11.8	5.32	12.4
November	v (m/s)	22.7	26.2	22.3	25.4
	γ (°)	8.46	15.8	9.55	15.1
Total	v (m/s)	31.8	34.5	29.9	32.9
	γ (°)	7.93	14.3	9.90	16.8

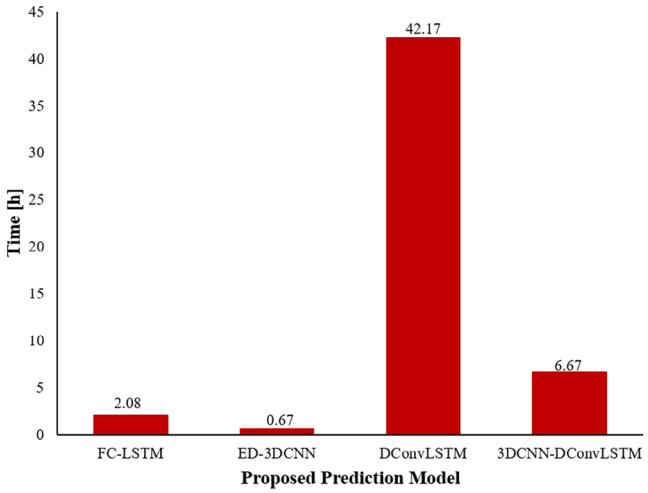

Fig. 10. Training time for all proposed forecasting models

4. Conclusion

This paper applied deep learning-based 3DCNN-DConvLSTM to wind speed and direction forecasting. For verifying effectiveness of the proposed 3DCNN-DConvLSTM model, RMSE, MAE, and MBE were used as evaluation indexes, and compared with FC-LSTM, ED-3DCNN, DConvLSTM, and persistent models. From simulation results, 3DCNN-DConvLSTM model had the highest forecasting accuracy. DConvLSTM and 3DCNN-DConvLSTM models could solve temporal sequence-caused convolutional structure and improve forecasting accuracy more than FC-LSTM and ED-3DCNN models. 3DCNN-DConvLSTM model which combine ED-3DCNN and DConvLSTM improved forecasting accuracy, more easy to training, and significantly reduced training time than DConvLSTM.

The future work is to improve forecasting accuracy of wind speed and direction uses more complex convolutional and increase data set that training, validation, and forecasting data set.

Table VIII. Forecasting time to forecast 1 h ahead

Proposed forecasting model	Forecasting time (min)
FC-LSTM	0.004
ED-3DCNN	0.001
DConvLSTM	0.072
DCNN-DConvLSTM	0.011

References

(1) IRENA: Global energy transformation a roadmap to 2050, www.irena.org, (2019).
(2) Sari AP, Suzuki H, Kitajima T, Yasuno T, Prasetya DA. Prediction model of wind speed and direction using deep neural network. *Journal of Electrical Engineering, mechatronic and Computer Science (JEEMECS)* 2020; **3**(1):1–10.
(3) Cali U, Sharma V. Short-term wind power forecasting using long-short term memory based recurrent neural network model and variable selection. *International Journal of Smart Grid and Clean Energy* 2019; **8**(2):103–110.
(4) Zhu Q, Chen J, Zhu L, Duan X, Liu Y. Wind speed prediction with spatio-temporal correlation: A deep learning approach. *Journal of Energies* 2018; **11**(4):705.
(5) J. Cao, D.J. Farnham, and U. Lall: Spatial-temporal wind field prediction by artificial neural networks, *arXiv* arXiv:1712.05293, (2017).
(6) Chen L, Li Z, Zhang Y. Multiperiod-ahead wind speed forecasting using deep neural architecture and ensemble learning. *Mathematical Problems in Engineering* 2019; **2019**:1–14.
(7) Marndi A, Patra GK, Gouda KC. Short-term forecasting of wind speed using time division ensemble of hierarchical deep neural networks. *Bulletin of Atmospheric Science and Technology* 2020; **1**:91–108.
(8) Hong YY, Martinez JJF, Fajardo AC. Day-ahead solar irradiation forecasting utilizing gramian angular field and convolutional long short-term memory. *IEEE access* 2020; **8**:18741–18753.
(9) R. Castro, Y.M. Souto, E. Ogasawara, F. Porto, and E. Bezerra: STConvS2S: Spatiotemporal convolutional sequence to sequence network for weather forecasting, *arXiv*: 1912.00134v4, (2020).
(10) Sari AP, Suzuki H, Kitajima T, Yasuno T, Prasetya DA, Rabi A. Deep convolutional long short-term memory for forecasting wind speed and direction. *SICE Journal of Control, Measurement, and System Integration (SICE JCMSI)* 2021; **14**(2):30–38.
(11) X. Shi, Z. Chen, H. Wang, D.Y. Yeung, W.K. Wong, and W.C. Woo: Convolutional LSTM network: A machine learning approach for precipitation nowcasting, *arXiv*, abs/1506.04214, pp. 1–9, (2015).
(12) A.P. Sari, H. Suzuki, T. Kitajima, T. Yasuno, D.A. Prasetya, and Nachrowie: Prediction model of wind speed and direction using convolutional neural network - long short term memory, *Proc. 2020 IEEE International Conference on Power and Energy (PECon)*, pp. 358–363, (2020).

(13) A.P. Sari, H. Suzuki, T. Kitajima, T. Yasuno, D.A. Prasetya, and A. Rabi': Prediction of wind speed and direction using encoding-forecasting network with convolutional long short-term memory. *Proc. 2020 59th Annual Conference of the Society of Instrument and Control Engineers (SICE)*, pp. 958–963, (2020).
(14) R. Yu, Z. Liu, X. Li, W. Lu, M. Yu, J. Wang, and B. Li: Scene learning: Deep convolutional networks for wind power prediction by embedding turbines into grid space, *arXiv*:1807.05666v2, (2018).
(15) Yasrab R. ECRU, an encoder-decoder based convolution neural network (CNN) for road-scene understanding. *Journal of Imaging* 2018; **4**(10):116.
(16) Zhang J, Florita A, Hodge B, Lu S, Hamann HF, Banunarayanan V, Brockway AM. A suite of metrics for assessing the performance of solar power forecasting. *Solar Energy* 2015; **111**:157–175.
(17) Rossi R. *Inventory Analytics*. Open Book Publishers: Cambridge; 2021.

Anggraini Puspita Sari (Student Member) received her B.E. and M.E. degrees from the University of Brawijaya, Malang, Indonesia in 2009 and 2012, respectively. Currently, she is pursuing Dr. Eng. degree at Tokushima University, Tokushima, Japan and is research about wind power prediction system. She is a lecturer in Electrical Engineering, the University of Merdeka Malang, Malang, Indonesia. She is a member of the Electrical Engineering Education Forum Indonesia (Fortei Indonesia) and a student member of the Institute of Electrical Engineers of Japan (IEEJ).

Hiroshi Suzuki (Member) received his Ph.D. degree from Tokushima University, Japan, in 2011. He is an Assistant Professor in the Faculty of Science and Technology, Tokushima University since 2016. His current research interests are intelligent control and sensor network. He is a member of the Institute of the Electrical Engineers of Japan (IEEJ), and the Society of Instrument and Control Engineers (SICE).

Takahiro Kitajima (Member) received his Dr. Eng. degree from Tokushima University, Japan in 2014. He is currently a technician with the Department of Electrical and Electronic Engineering, Tokushima University. His current research interests include the power output prediction of renewable energy and intelligent control systems of robots. He is a member of the Institute of Electrical and Electronics Engineers (IEEE), and the Institute of Electrical Engineers of Japan (IEEJ).

Takashi Yasuno (Member) received his Ph.D. degree from Tokushima University, Japan, in 1998. He is a Professor in the Faculty of Science and Technology, Tokushima University since 2013. His current research interest includes intelligent control of autonomous mobile robots, output prediction of wind power generation system, control engineering of rehabilitation system, agriculture support system. He is a member of the Society of Instrument and Control Engineers (SICE), the Institute of the Electrical Engineers of Japan (IEEJ), the Institute of Systems, Control and Information Engineers (ISCIE), the Robotics Society of Japan (RSJ), and the Institute of Electrical and Electronics Engineers (IEEE).

Dwi Arman Prasetya (Non-member) received his B.E. degree from Sepuluh Nopember Institute of Technology (ITS) in 2004. He received M.E. degree from University of Brawijaya, Malang, Indonesia in 2010. He received Dr. Eng. degree from Tokushima University, Tokushima, Japan in 2013. He is an Associate Professor in Electrical Engineering, the University of Merdeka Malang, Malang, Indonesia. His current research interest includes intelligent control of robotics and mechatronic system. He is a member of the Electrical Engineering Education Forum Indonesia (Fortei Indonesia), the Institute of Electrical and Electronics Engineers (IEEE), and Deputy head of the certification department of The Institution of Engineers Indonesia.

Rahman Arifuddin (Non-member) received his B.E. Degree from the National Institute of Technology Malang, Malang, Indonesia, in 2009. He received M.E. Degree from University of Brawijaya, Malang, Indonesia, in 2015. He is a lecturer in Electrical Engineering, the University of Merdeka Malang, Malang, Indonesia. His current research interests are the Instrument and control system. He is a member of the Electrical Engineering Education Forum Indonesia (Fortei Indonesia).